J|A|C|S ARTICLES

Published on Web 03/17/2010

# Exploring Resonance Levels and Nanostructuring in the PbTe−CdTe System and Enhancement of the Thermoelectric Figure of Merit

Kyunghan Ahn,[†] Mi-Kyung Han,[†] Jiaqing He,[‡] John Androulakis,[†] Sedat Ballikaya,[§,⊥] Ctirad Uher,[§] Vinayak P. Dravid,[‡] and Mercouri G. Kanatzidis*[,†]

*Department of Chemistry, Northwestern University, Evanston, Illinois 60208, Department of Materials Science and Engineering, Northwestern University, Evanston, Illinois 60208, Department of Physics, University of Michigan, Ann Arbor, Michigan 48109, and University of Istanbul, 34000 Vezneciler, Istanbul, Turkey*

Received December 21, 2009; E-mail: m-kanatzidis@northwestern.edu

***Abstract:*** We explored the effect of Cd substitution on the thermoelectric properties of PbTe in an effort to test a theoretical hypothesis that Cd atoms on Pb sites of the rock salt lattice can increase the Seebeck coefficient via the formation of a resonance level in the density of states near the Fermi energy. We find that the solubility of Cd is less than previously reported, and CdTe precipitation occurs to create nanostructuring, which strongly suppresses the lattice thermal conductivity. We present detailed characterization including structural and spectroscopic data, transmission electron microscopy, and thermoelectric transport properties of samples of PbTe−*x*% CdTe−0.055% $PbI_2$ ($x = 1, 3, 5, 7, 10$), PbTe−1% CdTe−*y*% $PbI_2$ ($y = 0.03, 0.045, 0.055, 0.08, 0.1, 0.2$), PbTe−5% CdTe−*y*% $PbI_2$ ($y = 0.01, 0.03, 0.055, 0.08$), and PbTe−1% CdTe−*z*% Sb ($z = 0.3, 0.5, 1, 1.5, 2, 3, 4, 5, 6$). All samples follow the Pisarenko relationship, and no enhancement of the Seebeck coefficient was observed that could be attributed to a resonance level or a distortion in the density of states. A maximum ZT of ∼1.2 at ∼720 K was achieved for the PbTe−1% CdTe−0.055% $PbI_2$ sample arising from a high power factor of ∼17 $\mu$W/(cm $K^2$) and a very low lattice thermal conductivity of ∼0.5 W/(m K) at ∼720 K.

## Introduction

Direct thermal-to-electric energy conversion using thermoelectric (TE) materials may result in energy efficiency improvements in a variety of areas where waste heat is abundant.[1,2] The dimensionless thermoelectric figure of merit, $ZT = (\sigma S^2 T)/\kappa$, defines the efficiency of a thermoelectric material, where $\sigma$ is the electrical conductivity, $S$ is the Seebeck coefficient (thermopower), $T$ is the absolute temperature, and $\kappa$ is the thermal conductivity. The recent advances reported in the performance of thermoelectric materials have been achieved mainly through remarkable reductions in the lattice thermal conductivity. These reductions have been the result of nanostructuring semiconductors such as PbTe[3−8] and $Bi_2Te_3$,[9] in which engineered nanoscale features strongly scatter acoustic phonons. One of the significant challenges moving forward is to understand how increases in the power factor ($\sigma S^2$) can be achieved that go beyond what is possible in the pristine semiconductors. One approach could be the introduction of so-called resonance states in the band near the Fermi level, which can produce enhancements in the Seebeck coefficient.[10,11]

A recent theoretical study suggested that resonance levels can be introduced in the conduction band when Cd is introduced on the metal sites of the PbTe rock salt structure, and correspondingly Tl can introduce resonance levels in the valence

[†] Department of Chemistry, Northwestern University.
[‡] Department of Materials Science and Engineering, Northwestern University.
[§] University of Michigan.
[⊥] University of Istanbul.

(1) (a) Bell, L. E. *Science* **2008**, *321*, 1457–1461. (b) Nolas, G. S.; Poon, J.; Kanatzidis, M. G. *MRS Bull.* **2006**, *31*, 199–205. (c) Kanatzidis, M. G. *Chemistry of Materials* **2010**, *22*, 648–659.
(2) (a) Snyder, G. J.; Toberer, E. S. *Nat. Mater.* **2008**, *7*, 105–114. (b) Sootsman, J. R.; Chung, D. Y.; Kanatzidis, M. G. *Angew. Chem., Int. Ed.* **2009**, *48*, 8616–8639.
(3) Hsu, K. F.; Loo, S.; Guo, F.; Chen, W.; Dyck, J. S.; Uher, C.; Hogan, T.; Polychroniadis, E. K.; Kanatzidis, M. G. *Science* **2004**, *303*, 818–821.
(4) (a) Poudeu, P. F. P.; D'Angelo, J.; Downey, A. D.; Short, J. L.; Hogan, T. P.; Kanatzidis, M. G. *Angew. Chem., Int. Ed.* **2006**, *45* (23), 3835–3839. (b) Poudeu, P. F. P.; Gueguen, A.; Wu, C. I.; Hogan, T.; Kanatzidis, M. G. *Chem. Mater.* **2010**, *22*, 1046–1053.
(5) (a) Androulakis, J.; Hsu, K. F.; Pcionek, R.; Kong, H.; Uher, C.; D'Angelo, J. J.; Downey, A.; Hogan, T.; Kanatzidis, M. G. *Adv. Mater.* **2006**, *18* (9), 1170–1173. (b) Poudeu, P. F. P.; Gueguen, A.; Wu, C. I.; Hogan, T.; Kanatzidis, M. G. *Chem. Mater.* **2010**, *22*, 1046–1053.
(6) Androulakis, J.; Lin, C.-H.; Kong, H.-J.; Uher, C.; Wu, C.-I.; Hogan, T.; Cook, B. A.; Caillat, T.; Paraskevopoulos, K. M.; Kanatzidis, M. G. *J. Am. Chem. Soc.* **2007**, *129* (31), 9780–9788.
(7) Sootsman, J. R.; Kong, H.; Uher, C.; D'Angelo, J. J.; Wu, C.-I.; Hogan, T. P.; Caillat, T.; Kanatzidis, M. G. *Angew. Chem., Int. Ed.* **2008**, *47* (45), 8618–8622.
(8) Zhou, M.; Li, J.-F.; Kita, T. *J. Am. Chem. Soc.* **2008**, *130* (13), 4527–4532.
(9) Poudel, B.; Hao, Q.; Ma, Y.; Lan, Y.; Minnich, A.; Yu, B.; Yan, X.; Wang, D.; Muto, A.; Vashaee, D.; Chen, X.; Liu, J.; Dresselhaus, M. S.; Chen, G.; Ren, Z. *Science* **2008**, *320*, 634–638.
(10) Ahmad, S.; Hoang, K.; Mahanti, S. D. *Phys. Rev. Lett.* **2006**, *96*, 056403.
(11) Ahmad, S.; Mahanti, S. D.; Hoang, K.; Kanatzidis, M. G. *Phys. Rev. B* **2006**, *74*, 155205.

  

band, which can lead to a significant enhancement in the electronic density of states (DOS).[10–12] Most recently, an experimental work of Heremans et al.[13] reported that values of ZT for p-type $Tl_{0.02}Pb_{0.98}Te$ reach 1.5 at 773 K because of enhancements in the Seebeck coefficient through a distortion of DOS in the valence band. The substitution of Cd in PbTe is predicted to result in a distortion in the DOS near the bottom of the conduction band.[11] If a resonance level is present near the Fermi energy, we expect to observe an enhancement in the Seebeck coefficient for a particular carrier concentration compared to a corresponding system lacking the resonance level. To be an effective resonance level however, the added metal center (e.g., Cd) in the lattice should be in a sufficiently high concentration so that it creates an extended state that is coupled to the conduction band, rather than a localized noninteracting state. In addition, a low lattice thermal conductivity may be realized through nanostructuring by the precipitation of excess CdTe when the solid solubility limit of CdTe in PbTe is reached according to the PbTe−CdTe pseudobinary phase diagram.[14]

Because Cd is isovalent with Pb, it is neither a donor nor an acceptor level in PbTe, and therefore in order to tune the Fermi energy, we also introduced n-type dopants (e.g., $PbI_2$ or Sb). We studied the thermoelectric properties of PbTe−$x$% CdTe as a function of $x$ and dopant concentration and looked for trends and enhancements that would be consistent with the theoretical predictions that Cd resonance levels can be introduced in the band structure. We present detailed investigations of structural properties, spectroscopic measurements, and transmission electron microscopy (TEM) as well as transport property investigations including electrical conductivity, Seebeck coefficient, Hall effect, and thermal conductivity on samples of PbTe−$x$% CdTe−0.055% $PbI_2$ ($x$ = 1, 3, 5, 7, 10), PbTe−1% CdTe−$y$% $PbI_2$ ($y$ = 0.03, 0.045, 0.055, 0.08, 0.1, 0.2), PbTe−5% CdTe−$y$% $PbI_2$ ($y$ = 0.01, 0.03, 0.055, 0.08), and PbTe−1% CdTe−$z$% Sb ($z$ = 0.3, 0.5, 1, 1.5, 2, 3, 4, 5, 6). An enhancement in ZT to ∼1.2 at ∼720 K is observed, and its origins are discussed.

## Experimental Section

**Synthesis.** For the preparation of samples of PbTe−$x$ mol % CdTe−0.055 mol % $PbI_2$ ($x$ = 1, 3, 5, 7, 10), PbTe−1 mol % CdTe−$y$ mol % $PbI_2$ ($y$ = 0.03, 0.045, 0.055, 0.08, 0.1, 0.2), PbTe−5 mol % CdTe−$y$ mol % $PbI_2$ ($y$ = 0.01, 0.03, 0.055, 0.08), and PbTe−1 mol % CdTe−$z$ mol % Sb ($z$ = 0.3, 0.5, 1, 1.5, 2, 3, 4, 5, 6) lead (Rotometals, 99.99%), cadmium (shot, 99.999%), antimony (shot, 99.999%), tellurium (Atlantic Metals, 99.999%), and lead iodide (Aldrich, 99.999%) were combined in an appropriate molar ratio in a 8 mm diameter graphite crucible, which was inserted in a 13 mm diameter fused silica tube. The tube was then evacuated and sealed under a residual pressure of $\sim 1 \times 10^{-4}$ Torr. For a typical experiment the following amounts were used: Pb (6.1401 g, 29.634 mmol), Cd (0.0333 g, 0.296 mmol), Te (3.8191 g, 29.930 mmol), and $PbI_2$ (0.0075 g, 0.016 mmol) were used to prepare 10 g of PbTe−1 mol % CdTe−0.055 mol % $PbI_2$.

The silica tube was heated at 1323 K for 5 h and cooled to 1023 K in 2 h. After standing at 1023 K for 4 h, the tube was cooled to room temperature over 12 h. Dense ingots were obtained with a dark silvery metallic shine. The ingots are stable in water and air and are strong enough to survive cutting and polishing.

**Powder X-ray Diffraction and Infrared Spectroscopy.** Powder X-ray diffraction patterns for samples of PbTe−$x$% CdTe−0.055% $PbI_2$ ($x$ = 1, 3, 5, 7, 10) and PbTe−1% CdTe−$z$% Sb ($z$ = 1, 2, 3, 4, 5, 6) were collected using Cu Kα radiation on an INEL diffractometer equipped with a position-sensitive detector and operating at 40 kV and 20 mA. Room-temperature optical diffuse reflectance measurements were performed using a Nicolet 6700 FTIR spectrometer in order to probe optical energy band gaps. This system was described elsewhere.[15]

**Thermal Conductivity.** The thermal diffusivity ($D$) was directly measured under a nitrogen atmosphere, and the specific heat ($C_p$) was indirectly derived using a standard sample (Pyroceram) as a function of temperature from room temperature to ∼720 K using the flash diffusivity method in a NETZSCH LFA 457 MicroFlash instrument. In the flash diffusivity method, the front face of a disk-shaped sample (∼8 mm diameter and 1−2 mm thickness) is irradiated by a short laser burst, and the resulting rear face temperature rise is recorded and analyzed by an IR detector. The thermal conductivity ($\kappa$) was calculated from the equation $\kappa = DC_p\rho$, where $\rho$ is the density of the sample, measured using sample dimensions and mass.

**Electrical Properties.** The samples for electrical properties measurement were cut and polished into a rectangular shape of ∼3 mm × 3 mm × 9 mm. The longer direction coincides with the direction in which the thermal conductivity is measured. The electrical conductivity $\sigma$ and Seebeck coefficient $S$ were measured simultaneously under a helium atmosphere (∼0.1 atm) from room temperature to ∼720 K using a ULVAC-RIKO ZEM-3 system.

**Hall Measurements.** The Hall coefficient was measured by using a homemade high-temperature apparatus, which provides a working range from 300 to ∼873 K. The sample was press mounted and protected with argon gas to avoid possible oxidization at high temperature. The Hall resistance was monitored with a Linear Research AC Resistance Bridge (LR-700), with constant magnetic fields of ±1 T applied by using an Oxford Superconducting magnet.

**High-Resolution Transmission Electron Microscopy (HRTEM).** The TEM samples were prepared by polishing, dimpling, and ion milling with liquid nitrogen to obtain thin specimens for analysis. Transmission electron microscope investigations were carried out in a JEOL 2100F microscope.

## Results and Discussion

**Powder X-ray Diffraction and Band Gaps.** The powder X-ray diffraction patterns of samples of PbTe −$x$% CdTe−0.055% $PbI_2$ ($x$ = 1, 3, 5, 7, 10) and PbTe−1% CdTe−$z$% Sb ($z$ = 1, 2, 3, 4, 5, 6) are shown in Figure 1(a) and (b), respectively. The samples crystallize in the NaCl-type structure without any noticeable second phase, Figure 1(a). The metallic radius[16] of Pb (1.750 Å) is larger than those of Cd (1.568 Å) and Sb (1.571 Å), and thus a small lattice contraction is expected with Cd and/or Sb incorporation. The refined lattice parameters for $x$ = 1, 3, 5, 7, and 10 are 6.466(1), 6.454(1), 6.451(1), 6.455(1), and 6.454(1) Å, respectively. This indicates that there is a maximum solid solubility limit of ∼3% CdTe in PbTe because of nearly constant lattice parameters above $x$ = 3, which is consistent with previous studies.[17,18] This solubility limit is however overestimated, as we will show below using TEM

(12) (a) Nemov, S. A.; Ravich, Yu. I. *Phys.-Usp.* **1998**, *41* (8), 735–759. (b) Volkov, B. A.; Ryabova, L. I.; Khokhlov, D. R. *Phys.-Usp.* **2002**, *45* (8), 819–846.
(13) Heremans, J. P.; Jovovic, V.; Toberer, E. S.; Saramat, A.; Kurosaki, K.; Charoenphakdee, A.; Yamanaka, S.; Snyder, G. J. *Science* **2008**, *321*, 554–557.
(14) Leute, V.; Schmidt, R. *Z. Phys. Chem.* **1991**, *172*, 81.
(15) Han, M.-K.; Hoang, K.; Kong, H.; Pcionek, R.; Uher, C.; Paraskevopoulos, K. M.; Mahanti, S. D.; Kanatzidis, M. G. *Chem. Mater.* **2008**, *20* (10), 3512–3520.
(16) Teatum, E. T.; Gschneidner, Jr., K. A.; Waber, J. T. *Compilation of calculated data useful in predicting metallurgical behavior of the elements in binary alloy systems*; Los Alamos Scientific Laboratory Report No. LA-4003; National Technical Information Service, U.S. Department of Commerce: Springfield, VA, 1968.
(17) Crocker, A. J. *J. Mater. Sci.* **1968**, *3*, 534–539.
(18) Sealy, B. J.; Crocker, A. J. *J. Mater. Sci.* **1973**, *8*, 1731–1737.

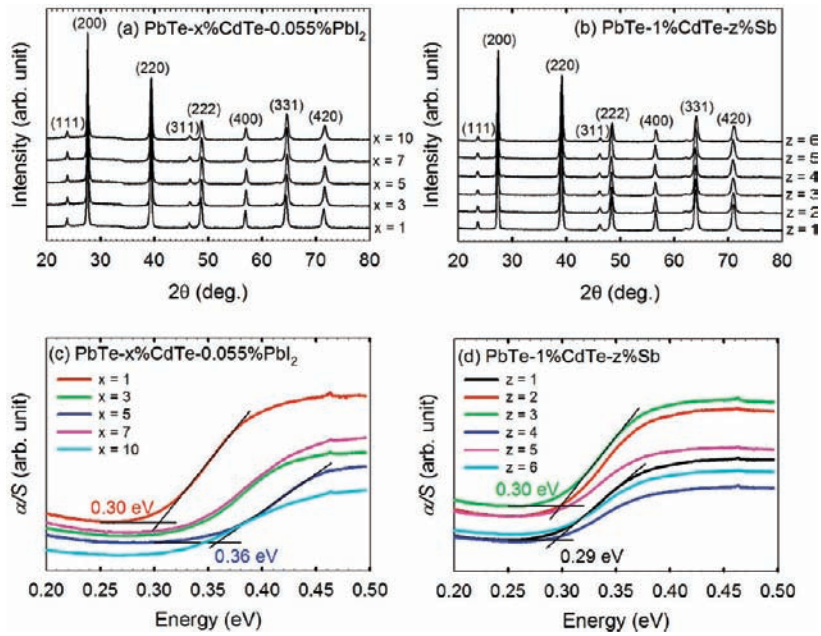


***Figure 1.*** (a) Powder X-ray diffraction patterns of samples of PbTe−$x$% CdTe−0.055% $PbI_2$ ($x$ = 1, 3, 5, 7, 10) and (b) PbTe−1% CdTe−$z$% Sb ($z$ = 1, 2, 3, 4, 5, 6), and (c) infrared absorption spectra and energy band gaps of samples of PbTe−$x$% CdTe−0.055% $PbI_2$ ($x$ = 1, 3, 5, 7, 10) and (d) PbTe−1% CdTe−$z$% Sb ($z$ = 1, 2, 3, 4, 5, 6).

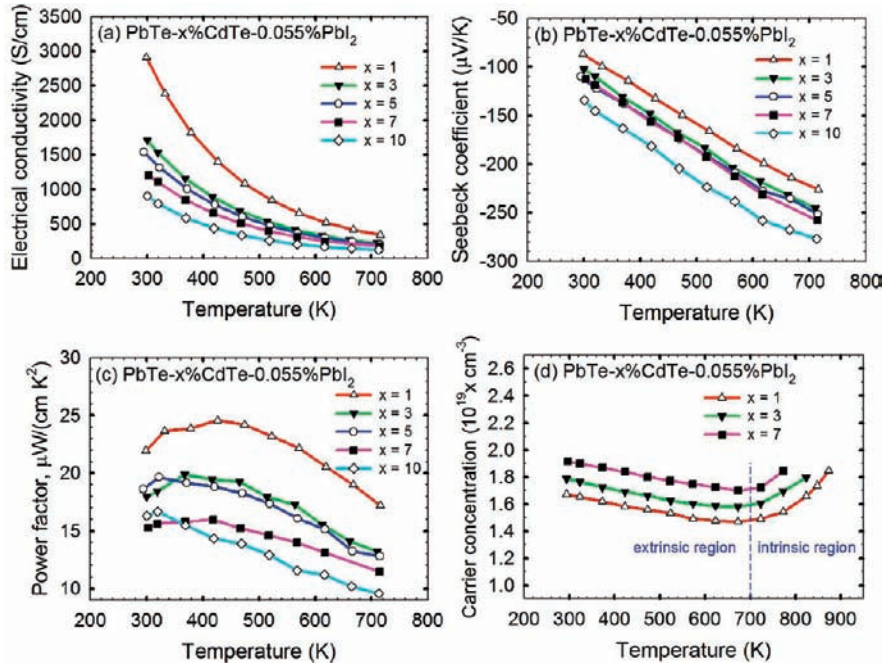


***Figure 2.*** Temperature dependence of (a) electrical conductivity, (b) Seebeck coefficient, (c) power factor, and (d) carrier concentration of samples of PbTe−$x$% CdTe−0.055% $PbI_2$ ($x$ = 1, 3, 5, 7, 10).

studies. The diffraction peaks from CdTe (zincblende, ZnS-type) should be observed for $x$ = 5, 7, and 10 in Figure 1(a), but they were not seen because all Bragg peaks of the ZnS-type phase ($a$ = 6.4809 Å) overlap with those of the NaCl phase. However, as shown Figure 1(b), the powder X-ray diffraction patterns for the Sb-containing samples indicate that there is a small Sb peak around 28 deg even in the 1% Sb sample, and this is consistent with the low solubility of Sb in PbTe.[19]

Typical infrared absorption spectra for samples of PbTe−$x$% CdTe−0.055% $PbI_2$ ($x$ = 1, 3, 5, 7, 10) and PbTe−1% CdTe−$z$% Sb ($z$ = 1, 2, 3, 4, 5, 6) are shown in Figure 1(c) and (d). In Figure 1(c), all samples exhibit spectroscopically observable energy band gaps between 0.30 and 0.36 eV compared to ∼0.29 eV of pure PbTe. The slightly higher band gap of PbTe−CdTe samples can be attributed to both the wider band gap of CdTe (1.56 eV) and more ionic character in the Cd−Te bond than the Pb−Te bond. For the Sb-containing samples in Figure 1(d) they show nearly constant energy band

(19) Henger, G. W.; Peretti, E. A. *J. Less-Common Met.* **1965**, *8* (2), 124–135.

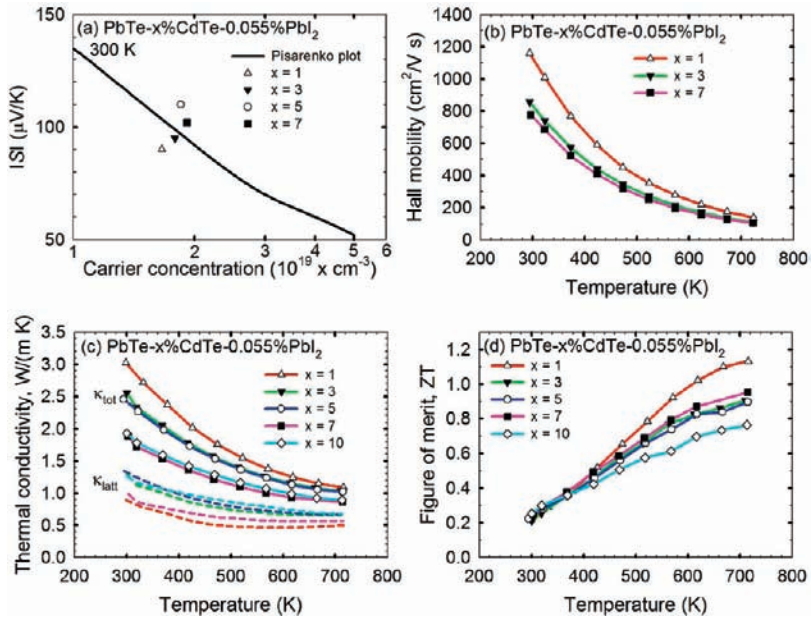


***Figure 3.*** (a) Absolute value of the thermopower of various samples ($x = 1, 3, 5, 7$) as a function of the carrier concentration on a logarithmic scale at room temperature. The solid line is the value calculated from the Pisarenko expression for n-type bulk PbTe with acoustic phonon scattering, (b) Hall mobility as a function of temperature of samples ($x = 1, 3, 7$), (c) temperature dependence of the total (solid line) and lattice (dash line) thermal conductivity, and (d) temperature dependence of the thermoelectric figure of merit of samples of PbTe−$x$% CdTe−0.055% $PbI_2$ ($x = 1, 3, 5, 7, 10$).

gap ranging between 0.29 and 0.30 eV regardless of Sb concentration.

**Effect on Thermoelectric Properties of CdTe Concentration in PbTe.** Figure 2(a) shows the temperature dependence of the electrical conductivity of samples of PbTe−$x$% CdTe−0.055% $PbI_2$ ($x = 1, 3, 5, 7, 10$). For all samples, the electrical conductivity decreases with increasing temperature, which is indicative of degenerate doping. The room-temperature electrical conductivities of samples with $x = 1, 3, 5, 7$, and 10 are ~2900, ~1700, ~1500, ~1200, and ~900 S/cm, respectively. As we will discuss below, the electrical conductivity decreases at higher CdTe concentration mainly because of the reduction in mobility. The electrical conductivity of the samples follows a nearly quadratic temperature-dependent power law of $\sigma \approx T^{-\delta}$ ($\delta = 2.1-2.3$), which is typical for n-type PbTe samples where acoustic phonon scattering dominates at high temperature:[20] $\delta$ are 2.3, 2.2, 2.1, 2.1, and 2.3 for $x = 1, 3, 5, 7$, and 10, respectively.

The Seebeck coefficient of the samples is shown in Figure 2(b). All samples show negative Seebeck coefficients over the entire temperature range, indicating n-type conduction. The Seebeck coefficient follows a nearly linear temperature dependence, and the room-temperature Seebeck coefficients are around −90, −100, −110, −110, and −130 $\mu$V/K for $x = 1, 3, 5, 7$, and 10, respectively. Figure 2(c) shows the temperature-dependent power factors ($PF = \sigma S^2$) of samples. As the temperature rises, the power factor increases, reaches a maximum, and then falls. For instance, in the case of $x = 1$, the power factor starts from ~22 $\mu$W/(cm $K^2$) at room temperature, reaches a maximum of ~25 $\mu$W/(cm $K^2$) around 430 K, and then decreases to ~17 $\mu$W/(cm $K^2$) around 720 K. Power factors of ~17, ~13, ~13, ~11, and ~10 $\mu$W/(cm $K^2$) were reached around 720 K for $x = 1, 3, 5, 7$, and 10, respectively.

The doping levels of the samples were probed with Hall effect measurements. The Hall coefficients measured in the temperature range of 300−873 K were negative, indicative of *n*-type conduction and consistent with the negative Seebeck coefficients. Assuming a simple parabolic band and single carrier conduction in our analysis, the carrier concentration $n$ was determined from the relationship $n = 1/eR_H$, where $e$ is the electronic charge and $R_H$ is the Hall coefficient. Figure 2(d) shows temperature-dependent carrier concentrations of PbTe−$x$% CdTe−0.055% $PbI_2$ ($x = 1, 3, 7$). One may notice that their carrier concentrations slightly decrease until ~700 K and then go up. In principle, the carrier concentration should be temperature independent in the extrinsic region because all the electrons at the donor levels are excited to the conduction band and thus the majority carrier (electron) concentration should stay at an almost constant level. In the intrinsic region the carrier concentration may be temperature dependent because electrons are excited from the valence band to the conduction band and thus minority carriers (hole) start to affect the magnitude of $R_H$ according to eq 1.

$$|R_H| = \frac{1}{e}\frac{n\mu_n^2 - p\mu_p^2}{(n\mu_n + p\mu_p)^2} \text{ in the low magnetic field limit} \quad (1)$$

where $n$ is electron concentration, $p$ is hole concentration, $\mu_n$ is electron mobility, and $\mu_p$ is hole mobility. However, we do not think that the slight variation in carrier concentration between 300 and 700 K is within the experimental error of Hall coefficient. The Hall data have accuracy better than the size of the symbol in Figure 2(d). That temperature trend is real and is likely due to the fact that the system is not fully degenerate as an ordinary metal would be, and there may be some dependence on the nature of scattering. In PbTe-based samples above ~700 K intrinsic conduction may occur and change the Hall coefficient with temperature. The room-temperature carrier concentration is nearly constant regardless of CdTe concentration: ~$1.7 \times 10^{19}$ $cm^{-3}$ for $x = 1$, ~$1.8 \times 10^{19}$ $cm^{-3}$ for $x = 3$, and ~$1.9 \times 10^{19}$ $cm^{-3}$ for $x = 7$. Figure 3(a) shows the

(20) Allgaier, R. S.; Scanlon, W. W. *Phys. Rev.* **1958**, *111*, 1029–1037.

absolute value of the Seebeck coefficient of samples as a function of carrier concentration at room temperature. The solid line (Pisarenko line[21]) in Figure 3(a) is a Pisarenko plot for bulk PbTe, and most n-type and p-type bulk PbTe samples fall on this line.[22−24] Our samples fall near this line, and thus an enhancement in Seebeck coefficient that could be attributed to resonance levels was not observed.

The Hall mobility $\mu_H$ was derived from the equation $\mu_H = \sigma/ne$. The variation of the Hall mobility with temperature is shown in Figure 3(b). The room-temperature Hall mobilities of $x = 1$, 3, and 7 are high at ∼1200, ∼860, and ∼780 $cm^2/(V\ s)$, respectively. The mobility tends to decrease as the CdTe concentration increases because CdTe precipitates in the PbTe matrix play a role as electron scatterers. For comparison the mobility of PbTe with a carrier concentration of $5 \times 10^{18}$ $cm^{-3}$ is ∼1500 $cm^2/(V\ s)$ at 300 K.[25] The carrier-concentration-dependent mobility at a finite temperature for n-type PbTe samples is $\mu \approx n^{-1/3}$ at 77 K and $\mu \approx n^{-4/3}$ at 4.2 K.[26] The temperature-dependent mobility of PbTe−$x$% CdTe −0.055% $PbI_2$ ($x = 1$, 3, 7) follows a quadratic power law of $\mu \approx T^{-\lambda}$ ($\lambda = 2.1$), which is in good agreement with those of n-type PbTe samples.[27]

The temperature dependences of the total and lattice thermal conductivity of samples are plotted in Figure 3(c). For comparison, the lattice thermal conductivities of PbTe−0.055% $PbI_2$ and undoped PbTe−1% CdTe samples made by the same preparation condition are shown together in Figure 1s (Supporting Information). For $x = 1$, the total thermal conductivity $\kappa_{tot}$ is ∼3.0 W/(m K) at room temperature, and it decreases with increasing temperature, reaching ∼1.1 W/(m K) at ∼720 K. The $\kappa_{tot}$ is the sum of the electronic thermal conductivity $\kappa_{elec}$ and the lattice thermal conductivity $\kappa_{latt}$. The $\kappa_{elec}$ can be calculated from the Wiedemann−Franz law, $\kappa_{elec} = L_0\sigma T$, where the Lorenz number $L_0 = 2.45 \times 10^{-8}$ $V^2/K^2$ was taken at its full degenerate value.[28] Subtracting the electronic term from the total thermal conductivity one obtains an estimate of the lattice thermal conductivity of the samples. However, it is known that $L_0$ can be 20% lower at high temperature, where the reduced Fermi energy ($E_F/kT$) is small.[29] Overestimating the Lorenz number at high temperature results in higher the electronic thermal conductivity ($\kappa_{elec}$), and thus, in underestimating the lattice thermal conductivity ($\kappa_{latt}$) by ∼30%. Consequently, in this work it is possible the value of the lattice thermal conductivity especially at high temperature could be underestimated.

For all samples, the estimated room-temperature lattice thermal conductivities are in the range 0.9−1.9 W/(m K) compared to the value of ∼2.2 W/(m K) in PbTe[30] and that of ∼2.5 W/(m K) for the PbTe−0.055% $PbI_2$ sample in this work. Namely, the room-temperature $\kappa_{latt}$ was ∼0.9, ∼1.3, ∼1.3, ∼1.9, and ∼1.9 W/(m K) for $x = 1$, 3, 5, 7, and 10, respectively. The value for $x = 1$ is comparable to estimates on other PbTe nanostructured materials such as LAST-18,[15] PbTe−PbS,[6] and PbTe−Sb;[31] see Table 1. This implies that nanostructuring through CdTe precipitation in the PbTe−CdTe system may also be occurring and is effective in scattering phonons. This was confirmed by the TEM studies presented below. It is notable that the lowest lattice thermal conductivity was observed for the 1% CdTe sample. Figure 3(d) shows the thermoelectric figure of merit ZT as a function of temperature. The highest ZT of ∼1.2, ∼0.9, ∼0.9, ∼1.0, and ∼0.8 at ∼720 K were achieved for $x = 1$, 3, 5, 7, and 10, respectively. Especially, for $x = 1$ the ZT of ∼1.2 at ∼720 K is significantly higher and slightly higher compared to the corresponding ZT of ∼0.8 for

***Table 1.*** Comparison of the Lattice Thermal Conductivity of the PbTe−1% CdTe with bulk PbTe and Nanostructured PbTe Materials Such As LAST-18, PbTe−PbS, and PbTe−Sb

| compound | $\kappa_{latt}$ (W/m·K) at ∼300 K | $\kappa_{latt}$ (W/m·K) at ∼700 K |
|---|---|---|
| PbTe[a] | ∼2.2 | ∼1.0 |
| PbTe−1% CdTe | ∼0.9 | ∼0.5 |
| LAST-18[b] | ∼0.8 | ∼0.4 |
| $(Pb_{0.95}Sn_{0.05}Te)_{0.92}(PbS)_{0.08}$[c] | ∼0.4 | ∼0.4 |
| PbTe−2% Sb[d] | ∼0.8 | ∼0.7 |

[a] Ref 30. [b] Ref 15. [c] Ref 6. [d] Ref 31.

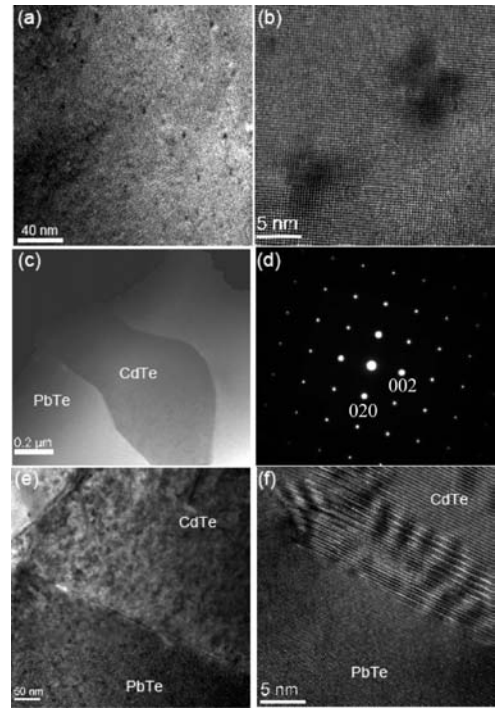


***Figure 4.*** (a) Low-magnification bright-field image of PbTe−1% CdTe showing CdTe precipitates with a dark contrast embedded in the PbTe matrix and (b) high-resolution lattice image clearly displaying matrix, precipitates, and their boundaries. (c) STEM image of PbTe−10% CdTe depicting a microscale CdTe precipitate in the PbTe matrix and (d) electron diffraction pattern including the large precipitate and matrix, which does not show split Bragg spots, suggesting very similar lattice parameters. (e) Low-magnification image of PbTe−10% CdTe sample showing two types (nanoscale and microscale) of CdTe precipitates. (f) Lattice image of boundary between the PbTe matrix and large CdTe precipitate.

(21) (a) Heremans, J. P.; Thrush, C. M.; Morelli, D. T. *J. Appl. Phys.* **2005**, *98*, 063703-1−063703-6. (b) Thiagarajan, S. J.; Jovovic, V.; Heremans, J. P. *Phys. Status Solidi RRL* **2007**, *1* (6), 256–258.
(22) Ioffe, A. F. *Semiconductor Thermoelements and Thermoelectric Cooling*; Infosearch Limited: London, 1957.
(23) Ioffe, A. F. *Physics of Semiconductors*; Infosearch Limited: London, 1960.
(24) Ravich, Yu. I.; Efimova, B. A.; Smirnov, I. A. *Semiconducting Lead Chalcogenides*; Plenum: New York, 1970.
(25) Tang, X. F.; Zhang, L. M.; Yuan, R. Z.; Chen, L. D.; Goto, T.; Hirai, T.; Dyck, J. S.; Chen, W.; Uher, C. *J. Mater. Res.* **2001**, *16* (12), 3343–3346.
(26) Kanai, Y.; Nii, R.; Watanabe, N. *J. Appl. Phys.* **1961**, *32*, 2146–2150.
(27) Joffe, A. F.; Stil'bans, L. S. *Rep. Prog. Phys.* **1959**, *22*, 167–203.
(28) Kittel, C. *Introduction to Solid State Physics*; John Wiley: New York, 1996.
(29) Harman, T. C.; Honig, J. M. *Thermoelectric and Thermomagnetic Effects and Applications*; McGraw-Hill: New York, 1967.
(30) Leute, V.; Volkmer, N. *Z. Phys. Chem. Neue Folge* **1985**, *144*, 145–155.
(31) Sootsman, J. R.; Pcionek, R. J.; Kong, H.; Uher, C.; Kanatzidis, M. G. *Chem. Mater.* **2006**, *18* (21), 4993–4995.

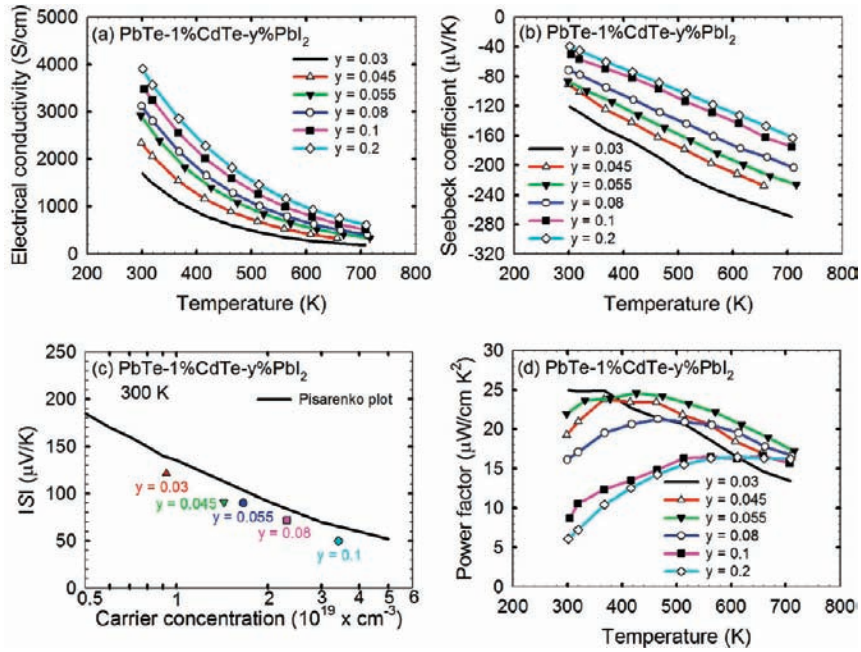


***Figure 5.*** (a) Temperature dependence of electrical conductivity, (b) Seebeck coefficient, (c) absolute value of the thermopower of various samples as a function of the carrier concentration on a logarithmic scale at room temperature, and (d) temperature dependence of power factor of samples of PbTe−1% CdTe−$y$% $PbI_2$ ($y$ = 0.03, 0.045, 0.055, 0.08, 0.1, 0.2).

optimized PbTe[2] and that of ∼1.1 recently reported for PbTe,[32] respectively. This improvement is mainly attributed to the low lattice thermal conductivity of ∼0.5 W/(m K) at ∼720 K and not to the power factor, which is normal for a PbTe-based material at this temperature.[32] For a control experiment, the ZT of a PbTe−0.055% $PbI_2$ sample made by the same preparation conditions was determined to be only ∼0.5.

**High-Resolution Transmission Electron Microscopy (HRTEM).** The significant reduction of lattice thermal conductivity in the PbTe−CdTe system should be due to the formation of CdTe nanoparticles inside the PbTe matrix. It is believed that embedded nanostructures in the bulk matrix can impact the enhanced thermoelectric performance through reduced lattice thermal conductivity.[3,9] TEM investigation of this system verified the presence of nanoscale precipitates in both the PbTe−1% CdTe and the PbTe−10% CdTe samples, but microscale precipitates only for the latter. Figure 4(a) shows a typical low-magnification image of the PbTe−1% CdTe sample, which depicts some inclusions with dark contrast and a size distribution of 2− 8 nm in the matrix. Figure 4(b) is a lattice image with two precipitates (dark spots) and clearly shows the coherent interface. The precipitates are presumably CdTe nanocrystals. The presence of nanocrystals inside the matrix should be the key for the strong suppression of the lattice thermal conductivity observed in the PbTe−1% CdTe sample in comparison to pure PbTe. These results suggest that the 3% solubility limit of CdTe in PbTe reported in the phase diagram is overestimated and the true limit is less than 1%. This highlights the dangers of using X-ray diffraction studies to determine solubility limits.

Figure 4(c) is a scanning transmission electron microscopy (STEM) image of the PbTe−10% CdTe sample that depicts a large dark CdTe precipitate in the PbTe matrix. The nanoscale precipitates at this magnification cannot be seen. Figure 4(d) is an electron diffraction pattern with the selected area aperture including the large precipitate and the PbTe matrix. From this diffraction pattern, we found no split spots, which is indicative of the precipitates having a similar crystal structure and very close lattice parameter to the matrix (coherent and endotaxial). Two types of CdTe precipitates (nanoscale and microscale) are clearly shown in a low-magnification TEM image (Figure 4(e)). In Figure 4(f) the lattice image shows atomic resolution level boundaries between the PbTe matrix and large CdTe precipitates. This image also shows modulated regions that arise simply from the overlap between the PbTe and CdTe lattices along the electron beam direction.

The nanoscale CdTe precipitates are dispersed evenly for the 1% CdTe sample, but for the 10% CdTe sample their size distribution ranges from nanometers to micrometers. The large micrometer size precipitates are believed not to contribute to any lattice thermal conductivity reduction, as the 10% CdTe sample exhibits a higher lattice thermal conductivity than the 1% CdTe sample.

**Effect on Thermoelectric Properties of $PbI_2$ Concentration in PbTe−$x$% CdTe ($x$ = 1, 5).** As shown above, the PbTe−1% CdTe sample showed a high ZT with a lower lattice thermal conductivity, but no significant enhancement in Seebeck coefficient that might be attributed to a resonance level was observed at the 0.055% $PbI_2$ concentration. According to the Mott equation 2[13,33]

$$S = \frac{\pi^2}{3}\left(\frac{k_B^2 T}{e}\right)\left(\frac{\mathrm{d}[\ln(\sigma(E))]}{\mathrm{d}E}\right)_{E=E_F} = \frac{\pi^2}{3}\left(\frac{k_B^2 T}{e}\right)\left(\frac{1}{n}\frac{\mathrm{d}n(E)}{\mathrm{d}E} + \frac{1}{\mu}\frac{\mathrm{d}\mu(E)}{\mathrm{d}E}\right)_{E=E_F} \quad (2)$$

where $k_B$ is the Boltzmann constant, $e$ is the electronic charge, $\sigma(E)$ is the energy-dependent electrical conductivity, $E_F$ is the

(32) Gelbstein, Y.; Dashevsky, Z.; Dariel, M. P. *Phys. B* **2005**, *363*, 196–205.

(33) (a) Cutler, M.; Mott, N. F. *Phys. Rev.* **1969**, *181*, 1336–1340. (b) Jonson, M.; Mahan, G. D. *Phys. Rev. B* **1980**, *21*, 4223–4229.

Fermi energy, $n(E)$ is the energy-dependent carrier concentration, and $\mu(E)$ is the energy-dependent mobility; the resonance level should be appropriately located around the Fermi level in order to significantly boost the Seebeck coefficient for a given carrier concentration. Thus, it is necessary to tune the carrier concentration of a sample to position the Fermi level near the resonance level. For this purpose, we investigated the thermoelectric properties of the samples of PbTe−1% CdTe−$y$% $PbI_2$ ($y$ = 0.03, 0.045, 0.055, 0.08, 0.1, 0.2). Also, we investigated doped samples of PbTe−5% CdTe−$y$% $PbI_2$ ($y$ = 0.01, 0.03, 0.055, 0.08) in order to probe if fractions of CdTe created resonance levels.

Figure 5(a) and (b) shows the temperature dependence of electrical conductivity and Seebeck coefficient of PbTe−1% CdTe−$y$% $PbI_2$ ($y$ = 0.03, 0.045, 0.055, 0.08, 0.1, 0.2), respectively. As expected, in Figure 5(a) the room-temperature electrical conductivity increases with increasing the $PbI_2$ concentration, which probably derives from the increase in the carrier concentration: ~1700 S/cm for $y$ = 0.03, ~2300 S/cm for $y$ = 0.045, ~2900 S/cm for $y$ = 0.055, ~3100 S/cm for $y$ = 0.08, ~3500 S/cm for $y$ = 0.1, and ~3900 S/cm for $y$ = 0.2. The temperature-dependent electrical conductivity follows a power law of $\sigma \approx T^{-\delta}$ ($\delta$ = 2.0 − 2.5): 2.5 for $y$ = 0.03, 2.3 for $y$ = 0.045, 2.3 for $y$ = 0.055, 2.2 for $y$ = 0.08, 2.1 for $y$ = 0.1, and 2.0 for $y$ = 0.2. In Figure 5(b), the absolute value of the room-temperature Seebeck coefficient decreases with increasing the $PbI_2$ concentration, which is consistent with their electrical conductivity data: −120 $\mu$V/K for $y$ = 0.03, −90 $\mu$V/K for $y$ = 0.045, −90 $\mu$V/K for $y$ = 0.055, −70 $\mu$V/K for $y$ = 0.08, −50 $\mu$V/K for $y$ = 0.1, and −40 $\mu$V/K for $y$ = 0.2.

The carrier concentrations of samples of PbTe−1% CdTe−$y$% $PbI_2$ ($y$ = 0.03, 0.045, 0.055, 0.08, 0.1) were probed with Hall effect measurements. Their room-temperature carrier concentrations are as follows: ~$0.9 \times 10^{19}$ $cm^{-3}$ for $y$ = 0.03, ~$1.4 \times 10^{19}$ $cm^{-3}$ for $y$ = 0.045, ~$1.7 \times 10^{19}$ $cm^{-3}$ for $y$ = 0.055, ~$2.3 \times 10^{19}$ $cm^{-3}$ for $y$ = 0.08, and ~$3.4 \times 10^{19}$ $cm^{-3}$ for $y$ = 0.1. In Figure 5(c), the absolute values of Seebeck coefficient of samples at 300 K versus carrier concentration are plotted with the so-called Pisarenko plot[22–24] in order to see whether the Seebeck coefficient of samples is enhanced at the same carrier concentration. Our samples nearly follow the Pisarenko plot, and thus it is clear that no significant enhancement in the room-temperature Seebeck coefficient is observed in the various $PbI_2$ concentrations. According to experimental data associated with In or Tl resonant levels,[12] dopants cease to act as donors (or acceptors) when their concentrations reach the point where Fermi level pinning is reached. Such a saturating behavior is not observed here. This is consistent with the lack of resonance level being present or being accessed at these carrier concentrations.

The corresponding temperature-dependent power factors of the PbTe−1% CdTe are shown in Figure 5(d). The power factor of $y$ = 0.03 decreases with increasing temperature, but those of $y$ = 0.045, 0.055, and 0.08 increase, reach a maximum, and then decrease with increasing temperature. For $y$ = 0.1 and 0.2, the power factor increases and saturates with increasing temperature. The room-temperature power factors of $y$ = 0.03, 0.045, 0.055, 0.08, 0.1, and 0.2 are ~25, ~19, ~22, ~16, ~9, and ~6 $\mu$W/(cm $K^2$), respectively. The respective power factors at ~720 K are ~13, ~16, ~17, ~17, ~16, and ~16 $\mu$W/(cm $K^2$).

Figure 6(a) and (b) shows the temperature dependence of electrical conductivity and Seebeck coefficient of PbTe−5% CdTe−$y$% $PbI_2$ ($y$ = 0.01, 0.03, 0.055, 0.08), respectively. The room-temperature electrical conductivity increases with increasing the $PbI_2$ concentration: ~200 S/cm for $y$ = 0.01, ~800 S/cm for $y$ = 0.03, ~1500 S/cm for $y$ = 0.055, and ~1800 S/cm for $y$ = 0.08. The temperature-dependent electrical conductivity follows a power law of $\sigma \approx T^{-\delta}$ ($\delta$ = 2.1−2.2): 2.2 for $y$ = 0.01, 2.2 for $y$ = 0.03, 2.1 for $y$ = 0.055, and 2.1 for $y$ = 0.08. In Figure 6(b), the absolute value of the room-temperature Seebeck coefficient decreases with increasing the $PbI_2$ concentration: −260 $\mu$V/K for $y$ = 0.01, −140 $\mu$V/K for $y$ = 0.03, −110 $\mu$V/K for $y$ = 0.055, and −90 $\mu$V/K for $y$ = 0.08. The corresponding temperature-dependent power factors are shown in Figure 6(c). The room-temperature power factors of $y$ = 0.01, 0.03, 0.055, and 0.08 are ~14, ~16, ~19, and ~14 $\mu$W/(cm $K^2$), respectively.

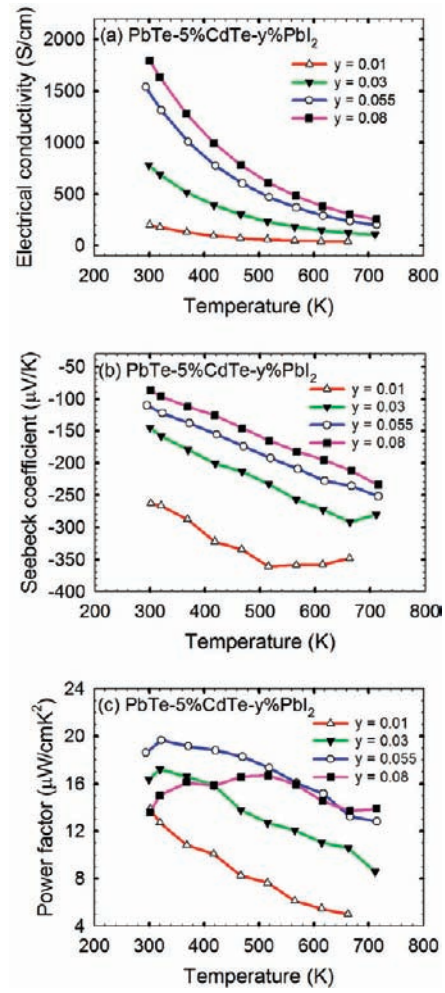


***Figure 6.*** (a) Temperature dependence of electrical conductivity, (b) Seebeck coefficient, and (c) power factor of samples of PbTe−5% CdTe−$y$% $PbI_2$ ($y$ = 0.01, 0.03, 0.055, 0.08).

Figure 7(a) shows the total and lattice thermal conductivity as a function of temperature for the PbTe−1% CdTe. The total thermal conductivity $\kappa_{tot}$ increases with increasing the $PbI_2$ concentration because of the electronic thermal conductivity $\kappa_{elec}$ contribution. In terms of the lattice thermal conductivity $\kappa_{latt}$, the $\kappa_{latt}$ at ~720 K converges to ~0.5 W/(m K) though the room-temperature $\kappa_{latt}$ is different for various $PbI_2$ concentrations. The temperature dependence of the figure of merit for the PbTe−1% CdTe is plotted in Figure 7(b). The ZT at ~720 K of $y$ = 0.045, 0.055, 0.08, 0.1, and 0.2 is ~1.1, ~1.2, ~1.0, ~0.8, and ~0.7, respectively. This indicates that the optimal $PbI_2$ doping of the

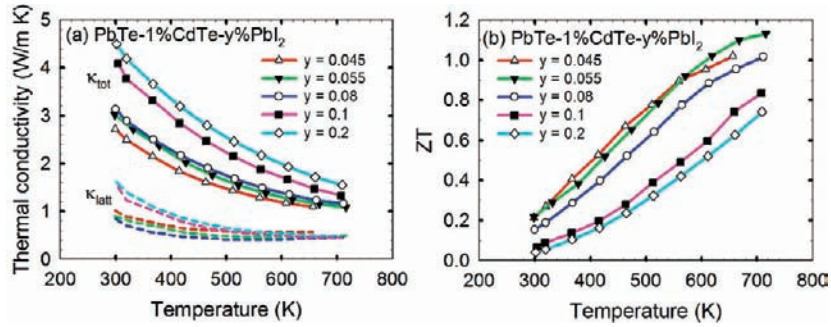


***Figure 7.*** (a) Temperature dependence of the total (solid line) and lattice (dash line) thermal conductivity and (b) the thermoelectric figure of merit of samples of PbTe−1% CdTe−$y$% $PbI_2$ ($y$ = 0.045, 0.055, 0.08, 0.1, 0.2).

PbTe−1% CdTe for best ZT is 0.055 mol %, though a Seebeck coefficient enhancement by resonance levels was not observed in various $PbI_2$ concentrations.

**Effect on Thermoelectric Properties of Sb Doping in PbTe−1% CdTe.** We attempted to tune the carrier concentration of PbTe−1% CdTe by Sb doping instead of $PbI_2$. Figure 8(a) and (b) shows the temperature dependence of electrical conductivity and Seebeck coefficient of PbTe−1% CdTe−$z$% Sb ($z$ = 0.3, 0.5, 1, 2, 4, 6). In Figure 8(a), as expected, the room-temperature electrical conductivity increases with increasing the Sb concentration until $z$ = 2, but then decreases with further higher Sb concentrations, which is probably due to the decrease in mobility above $z$ = 2: ∼1500 S/cm for $z$ = 0.3, ∼1900 S/cm for $z$ = 0.5, ∼2900 S/cm for $z$ = 1, ∼3900 S/cm for $z$ = 2, ∼3800 S/cm for $z$ = 4, and ∼3300 S/cm for $z$ = 6. The electrical conductivities of PbTe−1% CdTe−$z$% Sb ($z$ = 0.3, 0.5, 1, 2, 4) follow a nearly quadratic temperature-dependent power law of $\sigma \approx T^{-\delta}$ ($\delta$ = 1.9−2.4): 2.4 for $z$ = 0.3, 2.4 for $z$ = 0.5, 2.2 for $z$ = 1, 2.1 for $z$ = 2, and 1.9 for $z$ = 4. However, the power exponent of 6% Sb-containing sample is 1.6, which indicates that the higher Sb concentration causes the conductivity behavior to deviate from a quadratic power law probably due to either the transport behavior of the PbTe−CdTe system modified by excess antimony or a conductivity behavior of a mixed phase system. In Figure 8(b), the absolute value of the room-temperature Seebeck coefficient decreases with increasing Sb concentration, which confirms that the carrier concentration increases with increasing Sb concentration: −130 $\mu$V/K for $z$ = 0.3, −120 $\mu$V/K for $z$ = 0.5, −70 $\mu$V/K for $z$ = 1, −50 $\mu$V/K for $z$ = 2, −50 $\mu$V/K for $z$ = 4, and −40 $\mu$V/K for $z$ = 6. It seems that a Sb concentration of over 2% increases the carrier concentration while it decreases the mobility. The amphoteric nature of antimony as a dopant in PbTe has been recently reported,[34] but Sb appears to be an n-type dopant in the PbTe−CdTe system. Clearly, no significant enhancement in the room-temperature Seebeck coefficient consistent with a resonance level was observed at any Sb concentration.

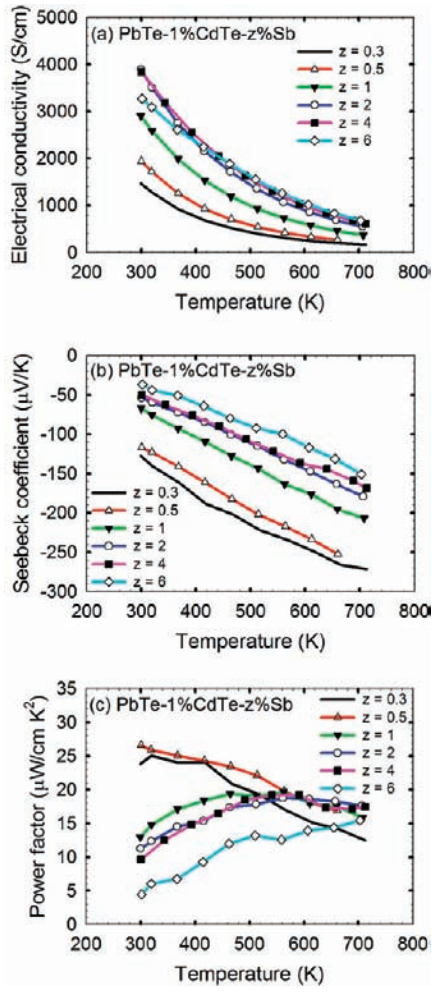


***Figure 8.*** (a) Temperature dependence of electrical conductivity, (b) Seebeck coefficient, and (c) power factor of samples of PbTe−1% CdTe−$z$% Sb ($z$ = 0.3, 0.5, 1, 2, 4, 6).

The corresponding power factors of PbTe−1% CdTe−$z$% Sb ($z$ = 0.3, 0.5, 1, 2, 4, 6) are shown in Figure 8(c). The power factors of $z$ = 0.3 and 0.5 decrease with increasing temperature, while those of $z$ = 1, 2, 4, and 6 increase with increasing temperature and saturation. The room-temperature power factors of $z$ = 0.3, 0.5, 1, 2, 4, and 6 are ∼24, ∼27, ∼13, ∼11, ∼10, and ∼4 $\mu$W/(cm K$^2$), respectively. The respective power factors at ∼720 K are ∼12, ∼16, ∼16, ∼18, ∼17, and ∼15 $\mu$W/(cm K$^2$).

Figure 9(a) shows the temperature dependence of the total and lattice thermal conductivity. The total thermal conductivity $\kappa_{tot}$ increases with increasing Sb concentration because of the contribution of electronic thermal conductivity. The lattice thermal conductivity $\kappa_{latt}$ derived from the Wiedemann−Franz law using the Lorenz number $L_0 = 2.45 \times 10^{-8}$ V$^2$/K$^2$ is plotted together in Figure 9(a). The $\kappa_{latt}$ at ∼720 K for $z$ = 0.5, 1, 2, 4, and 6 is ∼0.6, ∼0.6, ∼0.4, ∼0.6, and ∼0.7 W/(m K), respectively. The thermoelectric figure of merit, ZT, is shown

(34) Jaworski, C. M.; Tobola, J.; Levin, E. M.; Schmidt-Rohr, K.; Heremans, J. P. *Phys. Rev. B* **2009**, *80*, 125208-1–125208-10.

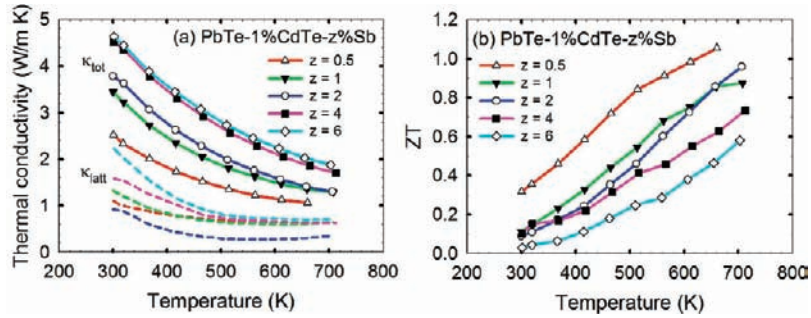


***Figure 9.*** (a) Temperature dependence of the total (solid line) and lattice (dash line) thermal conductivity and (b) the thermoelectric figure of merit of samples of PbTe−1% CdTe−z% Sb ($z = 0.5$, 1, 2, 4, 6).

in Figure 9(b). The ZT at ~720 K for $z = 0.5$, 1, 2, 4, and 6 is ~1.1, ~0.9, ~1.0, ~0.7, and ~0.6, respectively.

## Concluding Remarks

The thermoelectric properties of PbTe−CdTe samples were studied in detail in an effort to test theoretical predictions that Cd resonance levels can form in the conduction band, which could increase the Seebeck coefficient. No significant enhancement in the Seebeck coefficient was observed in various dopant concentrations ($PbI_2$ or Sb), which suggests that a resonance level either does not exist in the PbTe−CdTe system or was not accessed through the doping levels used in the present studies. The absence of a resonance level could be attributed to the low solubility of Cd in the Pb sublattice of PbTe, which was found to be <1% and much lower than the solubility limit reported in the PbTe−CdTe phase diagram. At such concentrations we presume that the Cd atoms are too far apart and form only localized levels near the bottom of the conduction band and not an extended resonance state that couples to it. Nevertheless, high-resolution transmission electron microscopy shows that well-developed nanostructuring is present in these materials arising from the nucleation and growth of CdTe nanocrystals and as a consequence of the low solubility of Cd. This plays an important role in reducing the lattice thermal conductivity. The moderate enhancement in ZT over PbTe achieved in the PbTe−CdTe system is mainly attributed to the low lattice thermal conductivity with no evidence for resonance levels being important.

**Acknowledgment.** Financial support from the Office of Naval Research (N00014-08-1-0613) is gratefully acknowledged. Transmission electron microscopy work was performed in the EPIC (NIFTI) (Keck-II) facility of NUANCE Center at Northwestern University. NUANCE Center is supported by NSF-NSEC, NSF-MRSEC, Keck Foundation, the State of Illinois, and Northwestern University. Work at the University of Michigan is supported by the Revolutionary Materials for Solid State Energy Conversion, an Energy Frontier Research Center funded by the U.S. Department of Energy, Office of Science.

**Supporting Information Available:** Graph of lattice thermal conductivities of doped PbTe and doped and undoped PbTe−CdTe materials. Tables of experimental and calculated values of heat capacity and density of PbTe−CdTe materials. This material is available free of charge via the Internet at http://pubs.acs.org.

JA910762Q